

Correlated topological pumping of interacting bosons assisted by Bloch oscillations

Wenjie Liu^{1,3}, Shi Hu⁴, Li Zhang^{1,3}, Yongguan Ke^{1,3,*} and Chaohong Lee^{1,2,3,†}

¹Guangdong Provincial Key Laboratory of Quantum Metrology and Sensing and School of Physics and Astronomy, Sun Yat-Sen University (Zhuhai Campus), Zhuhai 519082, China

²State Key Laboratory of Optoelectronic Materials and Technologies, Sun Yat-Sen University (Guangzhou Campus), Guangzhou 510275, China

³College of Physics and Optoelectronic Engineering, Shenzhen University, Shenzhen 518060, China

⁴School of Photoelectric Engineering, Guangdong Polytechnic Normal University, Guangzhou 510665, China

 (Received 22 August 2022; revised 29 November 2022; accepted 12 December 2022; published 17 January 2023)

Thouless pumping, not only achieving quantized transport but also immune to moderate disorder, has attracted growing attention in both experiments and theories. Here, we explore how particle-particle interactions affect topological transport in a periodically modulated and tilted optical lattice. Three characterized interaction effects are revealed: topological pumping of bound states, interaction blockade of scattering states, and topologically resonant tunnelings. Attributed to the tilting, we have found a linear scanning in the first Brillouin zone at each Bloch-oscillation period of multiparticle center-of-mass momentum. Not limited to multiparticle Wannier states, our scheme ensures a dispersionless quantized transport even for initial Gaussian-like wave packets of interacting bosons which do not uniformly occupy a given band. Our study deepens the understanding of correlation effects on topological states, and provides a feasible way for detecting topological properties in interacting systems.

DOI: [10.1103/PhysRevResearch.5.013020](https://doi.org/10.1103/PhysRevResearch.5.013020)

I. INTRODUCTION

Thouless pumping [1,2], a quantized transport in periodically modulated systems, can be viewed as a dynamical version of the integer quantum Hall effect. In Thouless pumping, when a uniform band occupation and adiabatic cyclic modulation are satisfied, the Chern number of the occupied band can be identified by the displacement per driven period. Due to its potential applications such as current standard, quantum state transfer, and entanglement generation, Thouless pumping has been theorized [3–8], and observed in ultracold atom [9–12], photon [13–15], and spin [16] systems. However, if the initial state is restricted to a single momentum state, a nonquantized geometric pumping has been observed in a Bose-Einstein condensate [17]. Recently, a new topological pumping assisted by Bloch oscillations is proposed, in which adding a tilting potential recovers a quantized transport of a single momentum state [18]. Owing to the tilting potential, two main obstacles in Thouless pumping, initial-state preparation with a uniform band occupation and wave-packet dispersion, are solved.

Since particle-particle interaction is ubiquitous and inevitable, Thouless pumping has been naturally generalized

to interacting systems [19–27]. Relying on cotranslational symmetry, Thouless pumping of a multiparticle Wannier state is related to the Chern number of the occupied multiparticle Bloch band. For few particles, the interactions support the Thouless pumping of bound states in which particles are transported as a whole [19,20], and topologically resonant tunnelings in which particles are transported one by one [21]. The interplay between the interaction strength and linear potential contributes to the engineering of the Floquet bands which can be identified by two-boson Thouless pumping [22]. For many particles, quantized topological pumping may occur in the Mott-insulating regime with one boson per unit cell [23] and break down due to the vanishing many-body energy gap [24,25]. On the other hand, the on-site interactions can be treated as Kerr nonlinearity in the mean-field approximation. Moderate nonlinearity supports quantized transport of a soliton, while strong nonlinearity makes the soliton localized, which has been observed in curved waveguide arrays [26,27]. Notice that a tilting potential has some advantages in topological pumping of a single particle. It is of great interest how the new topological pumping assisted by Bloch oscillations is affected by particle-particle interaction.

In this paper, we study topological transport of interacting bosons in a periodically driven and tilted optical superlattice, as depicted in Fig. 1. In a rotating framework, the tilting potential is transferred to the role of linearly varying phase in the tunneling rate, and multiparticle cotranslational symmetry is recovered. According to the multiparticle Bloch theorem, the energy bands consist of scattering-state bands and bound-state bands in strong interaction regions. Compared to the single-particle case with single-particle momentum in Ref. [18], we have demonstrated the multiparticle

*keyg@mail2.sysu.edu.cn

†lichah2@mail.sysu.edu.cn; chleecn@szu.edu.cn

Published by the American Physical Society under the terms of the [Creative Commons Attribution 4.0 International license](https://creativecommons.org/licenses/by/4.0/). Further distribution of this work must maintain attribution to the author(s) and the published article's title, journal citation, and DOI.

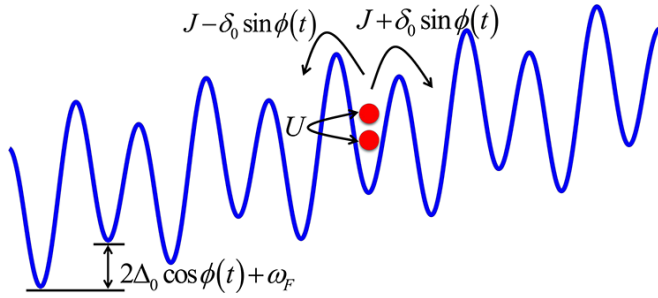


FIG. 1. Schematic of two bosons in a periodically driven superlattice under a tilted linear potential. The nearest-neighbor tunneling and on-site potential are driven via the phase $\phi(t)$. The on-site interaction is labeled by U and the tilt is ω_F .

center-of-mass momentum linearly scans the first Brillouin zone at each Bloch-oscillation period and clarified three main effects induced by interactions. The first is the topological pumping of bound states. For an initial bound state with an arbitrary center-of-mass momentum, we find that the center-of-mass displacement in an overall period is nearly quantized and independent of the initial quasimomentum, in contrast to nonquantized displacement in the absence of tilting potential. The quantization is related to a reduced Chern number defined as a one-dimensional time integral of the Berry curvature, which can be viewed as a perfect approximation of the two-body Chern number. We derive an effective single-particle model for the bound states by the many-body degenerate perturbation theory, and find the reduced Chern number of the single-particle model is consistent with the one mentioned above. The reduced Chern number can be used to precisely identify the boundary of topological phase transitions. The second is the interaction blockade of scattering states. For the scattering states, when the two particles are far away from each other and occupy the topologically nontrivial scattering-state bands, the two particles as a Fock state can be transferred as a whole. However, when the two particles occupy the topologically trivial scattering-state bands, the two counterpropagating particles can be independently shifted toward each other, incur an interaction blockade at the nearest-neighbor lattice sites, and come back to the initial state without crossing each other. The third is the topologically resonant tunnelings. When the interaction matches with the on-site potential difference between two nearest-neighbor sites, we find topologically resonant tunnelings occur where two particles move one by one.

This paper is organized as follows. In Sec. II, we introduce an interacting Rice-Mele model in a tilted optical lattice. In Sec. III, under the guidance of an effective single-particle model, we clarify the topological pumping of bound states assisted by Bloch oscillations. In Sec. IV, we show that the scattering states can be topologically transported as a whole or maintain the same after certain cycles, depending on the initial positions of the two particles. In Sec. V, we discuss the topologically resonant tunnelings assisted by Bloch oscillations when the on-site potential difference between nearest-neighbor sites compensates the interaction. In Sec. VI, we give a brief summary and discussion.

II. AN INTERACTING RICE-MELE MODEL IN A TILTED OPTICAL LATTICE

We consider an interacting Rice-Mele model with a tilted potential (see Fig. 1), described by the following Hamiltonian:

$$\begin{aligned} \hat{H}(t) = & \sum_j \{ [J + \delta_0 \sin[\pi j + \phi(t)]] \hat{a}_j^\dagger \hat{a}_{j+1} + \text{H.c.} \} \\ & + \frac{U}{2} \sum_j \hat{n}_j (\hat{n}_j - 1) + \sum_j \{ \Delta_0 \cos[\pi j + \phi(t)] \\ & + \omega_F j \} \hat{n}_j. \end{aligned} \quad (1)$$

Here, \hat{a}_j^\dagger (\hat{a}_j) creates (annihilates) a boson at site j with the atom number operator $\hat{n}_j = \hat{a}_j^\dagger \hat{a}_j$. For simplicity, we set the Planck constant $\hbar = 1$. J is the tunneling constant, and δ_0 and Δ_0 represent the modulation amplitudes of the tunneling strength and on-site potential, respectively. U denotes the interaction which can be tuned by the Feshbach resonance [28,29]. A double-well optical superlattice can be formed by a superposition of a short-wavelength optical lattice $V_s(t) = -V_s \cos^2(\pi x/d)$ with a period d and a long-wavelength optical lattice $V_l(t) = -V_l \cos^2[\pi x/(2d) - \phi(t)/2]$ with a period $2d$. The relative phase $\phi(t) = \phi_0 + \omega t$ has been experimentally realized [9,10].

ω_F is a tilt formed by applying a gradient magnetic field [30–35] or by placing the lattice along the gravitational field direction [36,37]. Considering magnetic field gradient as a tilt, atoms are prepared at hyperfine levels, and then the Zeeman shift occurs by applying a position-dependent magnetic field. The Zeeman energy gradient corresponds to a magnetic field gradient. In ultracold atomic experiments, a magnetic field gradient is applied to measure temperature [30], prepare arbitrary patterns of atoms [31], create state-dependent optical lattices [32], observe Bloch oscillations in position space [33,34], and obtain a tunneling phase [35]. After applying additional tilts along one [38,39] or two [40] directions in two-dimensional systems, the wave-packet centroid shifts are also proposed to dynamically detect the band topology. The tilt ω_F forms an on-site potential difference between two sites, which breaks the translational invariance of the lattice. To obtain the energy band under periodic boundary conditions, we apply a time-dependent unitary transformation $\hat{U} = \exp(i \sum_j j \omega_F t \hat{n}_j)$ to the Hamiltonian (1). The lattice translational invariance is recovered in the rotating frame given by

$$\begin{aligned} \hat{H}_{\text{rot}}(t) = & \frac{U}{2} \sum_j \hat{n}_j (\hat{n}_j - 1) + \sum_j \{ \Delta_0 \cos[\pi j + \phi(t)] \} \hat{n}_j \\ & + \sum_j \{ [J + \delta_0 \sin[\pi j + \phi(t)]] e^{-i\omega_F t} \hat{a}_j^\dagger \hat{a}_{j+1} \\ & + \text{H.c.} \}. \end{aligned} \quad (2)$$

Obviously, the tilted potential in the Hamiltonian (1) amounts to a time-dependent phase factor of the tunneling term in the rotating frame. The Hamiltonian (2) involves two frequencies where one is the modulation frequency ω depending on the parameter modulation period $T_m = 2\pi/\omega$ and the other is the tilt frequency ω_F depending on the tilt period $T_F = 2\pi/\omega_F$. p

and q are chosen as coprime numbers, and a rational number is defined as $\omega_F/\omega = p/q$. An overall period $T_{\text{tot}} = nqT_m$, as the common multiple of periods T_m and T_F , guarantees a translational symmetry in time domain for Hamiltonian (2) with $\hat{H}_{\text{rot}}(t + T_{\text{tot}}) = \hat{H}_{\text{rot}}(t)$ with $n = 1, 2, 3, \dots$. All eigenstates return to themselves over a period T_{tot} which is consistent with the period of Hamiltonian (2). In the following sections, the evolution time is chosen as T_{tot} .

We consider N interacting bosons in the optical superlattice consisting of L cells with d sites per cell. For Hamiltonian (2), particles as a whole satisfy a cotranslational invariance, that is, the system remains invariant as long as all the particles as a whole shift integer cells [21,41]. The quasimomentum of the center of mass, as a good quantum number, contributes to the multiparticle Bloch bands by solving the eigenequation

$$\hat{H}_{\text{rot}}(k)|\psi_m(k)\rangle = E_m(k)|\psi_m(k)\rangle. \quad (3)$$

Here, $|\psi_m(k)\rangle$ represents the multiparticle Bloch state with quasimomentum k in the m th multiparticle Bloch bands whose corresponding eigenvalue is $E_m(k)$. Combining the periodic parameters t and k , we can construct a closed surface where t serves as a quasimomentum in the second dimension [18,42,43]. Referring to real two-dimensional periodic systems [44], we define the Chern number in a two-dimensional closed surface as

$$C_m = \frac{1}{2\pi} \int_0^{2\pi/d} dk \int_0^{qT_m} dt \mathcal{F}_m(k, t) \quad (4)$$

with the Berry curvature of the m th band $\mathcal{F}_m = i(\langle \partial_t \psi_m | \partial_k \psi_m \rangle - \langle \partial_k \psi_m | \partial_t \psi_m \rangle)$.

Given $[\hat{H}_{\text{rot}}, \sum_j \hat{n}_j] = 0$, subspaces with different particle numbers are decoupled and the particle number is conserved. We mainly analyze the topological properties of two interacting bosons in the Rice-Mele model where the system is confined in two-boson basis $\{|l_1 l_2\rangle = (1 + \delta_{l_1 l_2})^{-1/2} \hat{a}_{l_1}^\dagger \hat{a}_{l_2}^\dagger |\mathbf{0}\rangle\}$ with $1 \leq l_1 \leq l_2 \leq L_t$ and $L_t = dL$ being the system size. After introducing $C_{l_1 l_2} = \langle \mathbf{0} | \hat{a}_{l_2} \hat{a}_{l_1} | \psi \rangle$, an arbitrary two-boson state can be expanded as $|\psi\rangle = \sum_{l_1 \leq l_2} \psi_{l_1 l_2} |l_1 l_2\rangle$ where $\psi_{l_1 l_2} = C_{l_1 l_2} (1 + \delta_{l_1 l_2})^{-1/2}$. Further, the eigenequation $\hat{H}_{\text{rot}}|\psi\rangle = E|\psi\rangle$ turns to

$$\begin{aligned} EC_{l_1 l_2} = & \{J + \delta_0 \sin[\pi l_1 + \phi(t)]\} e^{-i\omega_F t} C_{l_1+1, l_2} \\ & + \{J + \delta_0 \sin[\pi l_2 + \phi(t)]\} e^{-i\omega_F t} C_{l_1, l_2+1} \\ & + \{J + \delta_0 \sin[\pi(l_1 - 1) + \phi(t)]\} e^{i\omega_F t} C_{l_1-1, l_2} \\ & + \{J + \delta_0 \sin[\pi(l_2 - 1) + \phi(t)]\} e^{i\omega_F t} C_{l_1, l_2-1} \\ & + \{\Delta_0 \cos[\pi l_1 + \phi(t)] + \Delta_0 \cos[\pi l_2 + \phi(t)]\} C_{l_1 l_2} \\ & + UC_{l_1 l_2} \delta_{l_1 l_2}. \end{aligned} \quad (5)$$

III. TOPOLOGICAL PUMPING OF BOUND STATES ASSISTED BY BLOCH OSCILLATIONS

In this section we discuss the quantized topological pumping of two-boson bound states assisted by Bloch oscillations, where bosons tend to stay at the same site. By solving the two-particle eigenequation (3), we obtain two-particle Bloch bands [see Fig. 2(a)]. The parameters are chosen as $J = -1$, $\delta_0 = 0.8$, $\Delta_0 = 2$, $U = 30$, $\omega = 0.005$, $\phi_0 = 0$,

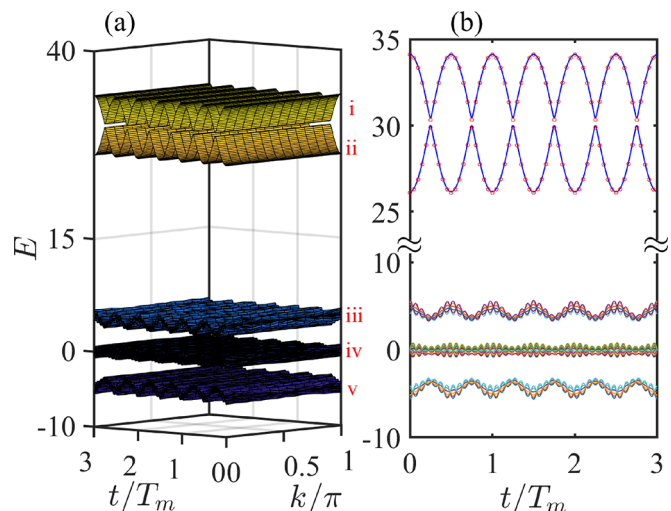


FIG. 2. Two-boson energy spectrum. (a) The 3D view of Bloch bands in the parameter space (k, t) . (b) The time evolution of energies $E(t)$ for Bloch states with $k = 0$. The red circles are the eigenenergies of the effective single-particle model (19). The parameters are chosen as $J = -1$, $\delta_0 = 0.8$, $\Delta_0 = 2$, $U = 30$, $\omega = 0.005$, $\phi_0 = 0$, $\omega_F/\omega = 10/3$, $L_t = 26$.

$\omega_F/\omega = 10/3$, $L_t = 26$. The two-particle energy spectrum consists of five isolated bands ordered for decreasing values of the energy marked with bands (i)–(v), of which the bands (i) and (ii) correspond to bound states and the remaining bands belong to scattering states. According to the definition (4), the Chern numbers of multiparticle Bloch bands are calculated: $C_i = -3$, $C_{ii} = 3$, $C_{iii} = -3$, $C_{iv} = 0$, and $C_v = 3$. The corresponding bulk-boundary correspondence under open boundary condition is presented in Appendix A. Figure 2(b) shows the change of energies for Bloch states with $k = 0$, where the band gaps remain open as time evolves.

The adiabatic transport theorem indicates that the velocity for a state with momentum k in the m th band is written to the first order as [45]

$$v_m(k, t) = \frac{\partial \varepsilon_m(k, t)}{\hbar \partial k} + \mathcal{F}_m(k, t), \quad (6)$$

which consists of dispersion of energy band and Berry curvature. After inputting a Bloch state, the pumping distance at the moment τ is determined by a semiclassical formula

$$\Delta X(\tau) = \int_0^\tau v_m(k, t) dt. \quad (7)$$

Without loss of generality, we pay attention to the band (ii) of the two-boson Bloch bands. Figure 3 displays the center-of-mass displacements of the multiparticle Bloch state at each quasimomentum in band (ii) after an evolution time $T_{\text{tot}} = 3T_m$. When $\omega_F = 0$, analogously to a geometric pumping [17], the center-of-mass displacements of Bloch states are associated with the quasimomentum k , whose amplitudes are significantly reduced by interaction. In the presence of ω_F , $\Delta X(3T_m)/d$ for each k are quite close to the Chern number ($C_{ii} = 3$), regardless of the interaction values. It implies that any states initially prepared on a given band can realize

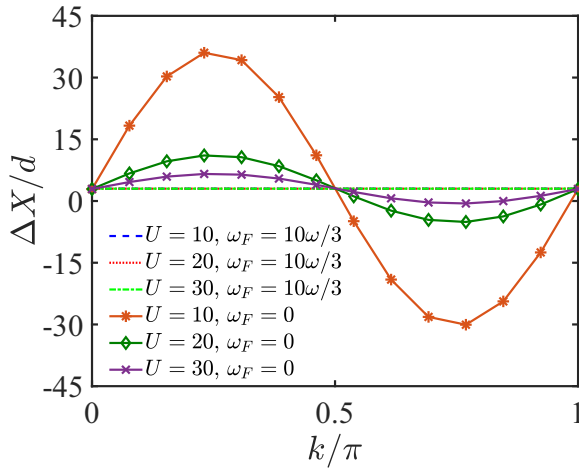


FIG. 3. The center-of-mass displacements of multiparticle Bloch states with different quasimomenta k in terms of the semiclassical formula (7) for different U and ω_F . The other parameters are chosen as $J = -1$, $\delta_0 = 0.8$, $\Delta_0 = 2$, $\omega = 0.005$, $\phi_0 = 0$.

a quantized topological pumping even for an initial single-momentum state.

In the two-particle basis, the multiparticle Bloch state is written as $|\psi\rangle = \sum_{l_1 \leq l_2} \psi_{l_1 l_2}(k_0, t_0) |l_1 l_2\rangle$ with the probability amplitude $\psi_{l_1 l_2}(k_0, t_0)$. Since multiparticle Bloch states are independent of k feature quantized transports, it is reasonable to predict that a quantized transport can be realized with an arbitrary wave packet initially prepared on a given band. To verify this, two typical initial states are considered. One is a strongly localized initial state in a real space, e.g., $|\psi(t_0)\rangle = |L_t/2, L_t/2\rangle$. The other is the Gaussian wave packet constructed by the multiparticle Bloch state with quasimomentum $k_0 = 0$ in band (ii), e.g.,

$$|\psi(t_0)\rangle = \sum_{l_1 \leq l_2} e^{-(l_1 - l_0)^2 + (l_2 - l_0)^2 / 4\sigma^2} \psi_{l_1 l_2}(k_0, t_0) |l_1 l_2\rangle. \quad (8)$$

Here, σ and l_0 are the width and center-of-mass position of the initial wave packet, respectively. Such a Gaussian wave packet (8) can be prepared by adding an additional harmonic potential. The evolved state $|\psi(t)\rangle = \sum_{l_1 \leq l_2} \psi_{l_1 l_2}(t) |l_1 l_2\rangle$ is determined by $|\psi(t)\rangle = \mathcal{T} \exp\{-i \int_{t_0}^t \hat{H}(t) dt\} |\psi(t_0)\rangle$ with the time-ordering operator \mathcal{T} . We extract the center-of-mass displacement

$$\Delta X(t) = X(t) - X(0) \quad (9)$$

from the particle density distribution $n_j(t) = \langle \psi(t) | \hat{n}_j | \psi(t) \rangle$ with $X(t) = \sum_{l_1 \leq l_2} \frac{l_1 + l_2}{2} |\psi_{l_1 l_2}(t)|^2$. The change of wave-packet width is given by

$$\Delta W(t) = W(t) - W(0) \quad (10)$$

with wave-packet width described by $W(t) = \sqrt{\sum_{l_1 \leq l_2} [(l_1 + l_2)/2 - X(t)]^2 |\psi_{l_1 l_2}(t)|^2}$.

By numerically calculating the wave-packet dynamics of different initial states and interaction strengths, we evaluate the effect of tilt in Fig. 4. Depending on the probability of initial states projecting onto band (ii) at time $t = 0$, the motion of a real-space wave packet undergoes distinct dynamics. The

tightly localized initial states $|\psi(t_0)\rangle = |L_t/2, L_t/2\rangle$ actually spread over bands (i) and (ii) at time $t = 0$, whose population probability in band (ii) at time $t = 0$ increases with interaction. As interaction increases, the bound-state bands (i) and (ii) gradually become flat with a reduced tunneling strength in a second-order tunneling process as derived in Eq. (18), accompanied by the initial Fock states becoming multiparticle Wannier states as an equal superposition of all the multiparticle Bloch states at each quasimomentum in band (ii) at time $t = 0$ (see Appendix B for initial multiparticle Wannier states). The center-of-mass displacement after $3T_m$ is extracted as displayed in Fig. 4. For $U = 10$, the population probability of the initial Fock state in band (ii) at time $t = 0$ is 0.858, both accompanied by nonquantized centroid displacements $2.644d$ ($\omega_F = 0$) in Fig. 4(a) and $2.607d$ ($\omega_F = 10\omega/3$) in Fig. 4(b). For $U = 30$, the centroid displacements of the initial Fock states are almost perfect quantization in Figs. 4(e) and 4(f) whose slight deviations are caused by the nonadiabatic transition for the smaller energy gap with a stronger interaction. The tilt ensures that the centroid position of the initial Gaussian wave packet shifts integer cells [see Figs. 4(d) and 4(h)]. Despite the lack of tilt, the centroid displacements of the initial Gaussian wave packet gradually approach to the band topology $C_{ii} = 3$ as interaction increases [see Figs. 4(c) and 4(g)]. In agreement with the semiclassical results in Fig. 3, this behavior is directly attributed to the reduced tunneling strength by the interaction. When applied to the tilting, the real-space wave-packet dynamics in Fig. 4(h) has a slight difference with the absence of the tilting in Fig. 4(g) due to the reduced tunneling strength by strong interaction, while the effect of tilt can be obviously observed in quasimomentum space in Appendix C.

It can be seen from Fig. 4 that the initial wave packets may spread over the whole lattice over enough time in the absence of tilt. However, in the presence of tilt, the initial wave packets are well localized with initial widths. This is because the wave-packet dispersion can be significantly suppressed by the tilt. We find that the role of a tilt ensures the dispersionless quantized centroid displacements once the initial states are prepared on a given band and follow adiabatic evolutions. While for the absence of tilt the quantized transports require the initial states uniformly filling at a specific band such as Wannier states with adiabatic driving. It is worth mentioning nonadiabatic effects also break the topological pumping. Whether the tilt is applied or not, the topological pumping after T_{tot} approaches the quantized value only if the adiabatic driving condition is satisfied. Fast topological pumping out of the adiabatic approximation is proposed by introducing the time-periodic dissipation [46] and mapping onto the zero curvature representation of the Euclidean sinh-Gordon equation [8].

A. Effective single-particle model

To have a better understanding of the bound-state transport mechanism, we take the interaction term as the domination and the other terms as the perturbation, and employ the many-body degenerate perturbation theory to analytically derive an effective single-particle model of bound states. The effective single-particle model can greatly describe the topological

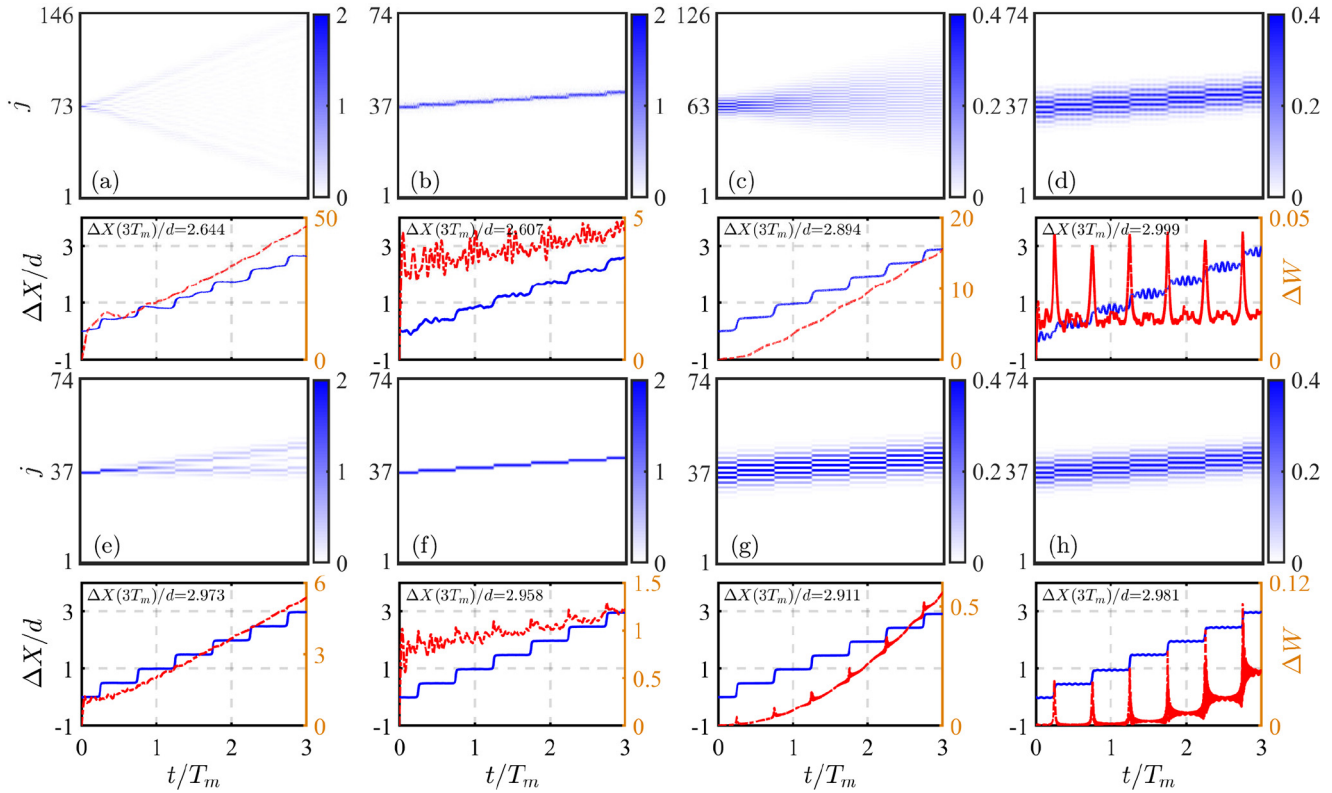


FIG. 4. The time evolution of particle density distribution of the bound-state dynamics. Blue lines and red dashed lines indicate the corresponding center-of-mass displacement $\Delta X(t)/d$ and variation of wave-packet width $\Delta W(t)$. Different interaction strengths are examined: (a)–(d) $U = 10$ and (e)–(h) $U = 30$. The role of tilt is analyzed: $\omega_F = 0$ (the first and third columns) and $\omega_F = 10\omega/3$ (the second and fourth columns). Two types of initial states are discussed: localized Fock states (the first and second columns) and extended Gaussian states (the third and fourth columns). The other parameters are chosen as $J = -1$, $\delta_0 = 0.8$, $\Delta_0 = 2$, $\omega = 0.005$, $\phi_0 = 0$, and $T_{\text{tot}} = qT_m = 3T_m$.

properties of bound-state bands, where eigenvalues, eigenstates, and topological invariants of the bound-state bands can be solved analytically. Consequently, the reduced Chern number of the multiparticle Bloch bands can be defined.

The Hamiltonian (1) is divided into two parts, $\hat{H}(t) = \hat{H}_0 + \hat{H}_{\text{int}}$ with

$$\hat{H}_{\text{int}} = \frac{U}{2} \sum_j \hat{n}_j(\hat{n}_j - 1) \quad (11)$$

as the interaction term and

$$\begin{aligned} \hat{H}_0 = & \sum_j \{ \{ J + \delta_0 \sin[\pi j + \phi(t)] \} \hat{a}_j^\dagger \hat{a}_{j+1} + \text{H.c.} \} \\ & + \sum_j \{ \Delta_0 \cos[\pi j + \phi(t)] + \omega_F j \} \hat{n}_j \end{aligned} \quad (12)$$

as the noninteraction term. In the strongly interacting regime $U \gg (J, \delta_0, \Delta_0, \omega_F)$, \hat{H}_0 is treated as a perturbation to \hat{H}_{int} . \hat{H}_{int} includes two degenerate subspaces \mathcal{U} and \mathcal{V} . The subspace \mathcal{U} consists of bound states with two bosons at the same site, that is, $\mathcal{U} \equiv \{|2\rangle_j\}$, and the degenerate energy is $E_j = U$. The subspace \mathcal{V} consists of states with two bosons at different sites, that is, $\mathcal{V} \equiv \{|1\rangle_j|1\rangle_k\}$, and the degenerate energy is $E_{jk} = 0$ with $j \neq k$. We respectively define the projection operators into the subspaces \mathcal{U} and \mathcal{V} as

$$\hat{P} = \sum_j |2\rangle_j \langle 2|_j \quad (13)$$

and

$$\hat{S} = \sum_{j \neq k} \frac{1}{E_j - E_{jk}} |1\rangle_j |1\rangle_k \langle 1|_k \langle 1|_j. \quad (14)$$

Using a second-order degenerate perturbation theory [47,48], the effective Hamiltonian in the subspace \mathcal{U} is given by

$$\hat{H}_{\text{eff}} = \hat{h}_0 + \hat{h}_1 + \hat{h}_2 = E_j \hat{P} + \hat{P} \hat{H}_0 \hat{P} + \hat{P} \hat{H}_0 \hat{S} \hat{H}_0 \hat{P}. \quad (15)$$

The zero-order term satisfies

$$\hat{h}_0 = E_j \hat{P} = U \sum_j |2\rangle_j \langle 2|_j. \quad (16)$$

The first-order term is

$$\hat{h}_1 = \hat{P} \hat{H}_0 \hat{P} = \sum_j \{ 2\Delta_0 \cos[\pi j + \phi(t)] + 2\omega_F j \} |2\rangle_j \langle 2|_j, \quad (17)$$

and the second-order term becomes

$$\begin{aligned} \hat{h}_2 = & \hat{P} \hat{H}_0 \hat{S} \hat{H}_0 \hat{P} \\ = & \sum_j \frac{2\{J + \delta_0 \sin[\pi j + \phi(t)]\}^2}{U} |2\rangle_j \langle 2|_{j+1} + \text{H.c.} \\ & + \left[\frac{2(J - \delta_0)^2}{U} + \frac{2(J + \delta_0)^2}{U} \right] \sum_j |2\rangle_j \langle 2|_j. \end{aligned} \quad (18)$$

Combining Eqs. (16), (17), and (18), the effective single-particle model yields

$$\hat{H}_{\text{eff}} = \sum_j \frac{2[J + \delta_0 \sin[\pi j + \phi(t)]]^2}{U} \hat{b}_j^\dagger \hat{b}_{j+1} + \text{H.c.} \\ + \sum_j \{2\Delta_0 \cos[\pi j + \phi(t)] + 2\omega_F j\} \hat{b}_j^\dagger \hat{b}_j + \mathcal{C}. \quad (19)$$

Here, \hat{b}_j^\dagger represents the creation of two bosons at the site j simultaneously, that is, $\hat{b}_j^\dagger|\mathbf{0}\rangle = |2\rangle_j$. Given the conservation of the particle number, \mathcal{C} is an energy constant with $\mathcal{C} = U + 2(J - \delta_0)^2/U + 2(J + \delta_0)^2/U$. Similarly, the tilted potential breaks the lattice translational invariance which can be recovered in the rotating frame as

$$\hat{H}_{\text{eff}}^{\text{rot}} = \sum_j \frac{2[J + \delta_0 \sin[\pi j + \phi(t)]]^2}{U} e^{-i2\omega_F t} \hat{b}_j^\dagger \hat{b}_{j+1} \\ + \text{H.c.} + \sum_j 2\Delta_0 \cos[\pi j + \phi(t)] \hat{b}_j^\dagger \hat{b}_j + \mathcal{C}. \quad (20)$$

B. The reduced Chern number of multiparticle bound-state bands

To obtain the eigenvalues and eigenstates of the bound-state bands in quasimomentum space, we take the Fourier transform for the effective single-particle model (20) as

$$\hat{b}_{2j}^\dagger = \frac{1}{\sqrt{L}} \sum_k e^{-ik2j} \hat{b}_{k,e}^\dagger, \\ \hat{b}_{2j-1}^\dagger = \frac{1}{\sqrt{L}} \sum_k e^{-ik(2j-1)} \hat{b}_{k,o}^\dagger. \quad (21)$$

Here k is the quasimomentum and L is the cell number. o (e) represents the odd (even) site. After the Fourier transform (21), the Hamiltonian (20) can be decomposed as $\hat{H}_{\text{eff}}^{\text{rot}}(t) = \sum_k \hat{H}_{\text{eff}}^{\text{rot}}(k, t)$. Each $\hat{H}_{\text{eff}}^{\text{rot}}(k, t)$ belongs to a two-level quantum system

$$\hat{H}_{\text{eff}}^{\text{rot}}(k, t) = h_x \hat{\sigma}_x + h_y \hat{\sigma}_y + h_z \hat{\sigma}_z + \mathcal{C}, \quad (22)$$

where

$$\begin{pmatrix} h_x \\ h_y \\ h_z \end{pmatrix} = \begin{pmatrix} 4 \frac{\{J^2 + \delta_0^2 \sin^2[\phi(t)]\}}{U} \cos(k - 2\omega_F t) \\ -4 \frac{\{2J\delta_0 \sin[\phi(t)]\}}{U} \sin(k - 2\omega_F t) \\ 2\Delta_0 \cos[\phi(t)] \end{pmatrix}. \quad (23)$$

By solving the eigenequation $\hat{H}_{\text{eff}}^{\text{rot}}(k, t)|u(k, t)\rangle = \varepsilon(k, t)|u(k, t)\rangle$, the eigenvalue is

$$\varepsilon_{\pm} = \pm \sqrt{h_x^2 + h_y^2 + h_z^2} + \mathcal{C}. \quad (24)$$

The eigenstate satisfies

$$|u_{\pm}(k, t)\rangle = \begin{pmatrix} h_x - ih_y \\ \varepsilon_{\pm} - h_z \\ 1 \end{pmatrix}. \quad (25)$$

Under the same parameters, the eigenvalue (24) is added in Fig. 2(b) with red circles, which agrees well with the two bound-state energies.

Based on the equivalent definition of the Berry curvature

$$\mathcal{F}_m(k, t) = -2 \text{Im} \left[\sum_{m' \neq m} \frac{\langle u_m | \partial_k \hat{H} | u_{m'} \rangle \langle u_{m'} | \partial_t \hat{H} | u_m \rangle}{(\varepsilon_m - \varepsilon_{m'})^2} \right] \quad (26)$$

with $m = \pm$, we derive the Berry curvatures of two bands in the effective single-particle model (20) as

$$\mathcal{F}_{\pm}(k, t) = 32 \frac{J\delta_0\omega\Delta_0}{U} \frac{\{J^2 + \delta_0^2 \sin^2[\phi(t)]\}}{U} \\ \times \frac{1 - \cos^2[\phi(t)] \cos^2(k - 2\omega_F t)}{[\varepsilon_{\pm}(k, t)]^3}. \quad (27)$$

The instantaneous eigenvalue $\varepsilon_{\pm}(k, t)$ as a periodic function of k and t ensures that the integration of the dispersion velocity in the semiclassical formula (7) is equal to zero. After an evolution time T_{tot} , only the integration over the time of the Berry curvature contributes to the center-of-mass displacement of the wave packet, which is defined as the reduced Chern number

$$C_{m,\text{red}}(qT_m) \equiv \frac{\Delta X(qT_m)}{d} = \frac{1}{d} \int_0^{qT_m} \mathcal{F}_m(k, t) dt. \quad (28)$$

The reduced Chern numbers obtained from Eqs. (27) and (28) yield the values 2.961 ($U = 10$) and 2.992 ($U = 30$). The other parameters are chosen as $J = -1$, $\delta_0 = 0.8$, $\Delta_0 = 2$, $\omega = 0.005$, $\omega_F = 10\omega/3$, $\phi_0 = 0$, and $T_{\text{tot}} = qT_m = 3T_m$. Compared with the band topology $C_{\text{ii}} = 3$, the slight deviation arises from the perturbation condition for the effective model (19). Given the validity of the effective model, the results become more accurate for a stronger interaction. It indicates that the bound-state topological properties can be well described by the effective model for enough interaction strength. In Appendix D, we have analytically derived a vital relationship $C_{m,\text{red}}(qT_m) = C_m$ between the reduced Chern number and the Chern number of the bound-state bands for $\omega_F/\omega \rightarrow \infty$.

C. Detecting topological phase transitions by the reduced Chern number

The measurement of topological invariants plays an important role in understanding topological phases. The band topology induces quantized transport, which may provide a way for detecting topological phase transitions in an interacting system. By solving degenerate points of two bound-state bands, the topological phase boundary without a tilt is analytically captured under the perturbation condition. There exists a quantum criticality at $\Delta_0 = 0$ ($\delta_0 = 0$) regardless of δ_0 (Δ_0). Except for the critical boundaries, the Chern number C_{ii} of the band (ii) is calculated in terms of Eq. (4), and the corresponding topological phase diagram is shown in Fig. 5(a). The parameters are chosen as $J = -1$, $\omega = 0.005$, $\omega_F = 0$, and $\phi_0 = 0$. The system size is $L_r = 58$.

We focus on the topological phase transition from $C_{\text{ii}} = -3$ to $C_{\text{ii}} = 3$ when Δ_0 takes a value from -2 to 2 at $\delta_0 = 0.8$, as shown in the red dashed lines in Figs. 5(a) and 5(b). The transition of the Chern number is sharper across the critical point $\Delta_0 = 0$. When the tilt is present, the reduced Chern number $C_{\text{ii,red}}$ in band (ii) is calculated by Eq. (28). The reduced Chern number can be used for detecting the critical

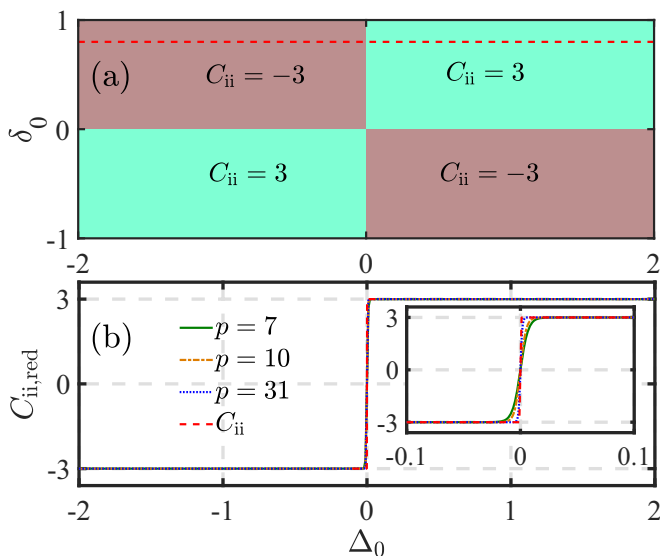


FIG. 5. (a) The Chern number C_{ii} of band (ii) with $\omega_F = 0$. (b) The detection of topological phase transition in terms of the Chern number C_{ii} with $\omega_F = 0$ and reduced Chern number $C_{ii,red}$ with $\omega_F = p\omega/q$. The inset is an enlarged part in (b). The other parameters are chosen as $J = -1$, $\omega = 0.005$, $\phi_0 = 0$, and $T_{tot} = qT_m = 3T_m$. The system size is $L_t = 58$.

point more accurately as the tilt ω_F increases, as shown in Fig. 5(b). Therefore, the reduced Chern number offers a flexible way for the detection of topological phase transitions in interacting systems.

IV. TOPOLOGICAL PUMPING OF SCATTERING STATES ASSISTED BY BLOCH OSCILLATIONS

The continuum band of scattering states is divided into three isolated cluster bands (iii)–(v). At the initial moment ($t/T_m = 0$), in band (v) two independent bosons mainly occupy different odd sublattices; in band (iv) one (the other) boson mainly occupies the odd (even) sublattice; and in band (iii) two independent bosons mainly occupy different even sublattices. Under the appropriate parameters ($J = -1$, $\delta_0 = 0.8$, $\Delta_0 = 7$, $U = 30$, $\omega = 0.05$, $\phi_0 = 0$, $\omega_F/\omega = 31/3$, $L_t = 58$), initial state $|\psi(t_0)\rangle = |21, 35\rangle$ ($|\psi(t_0)\rangle = |23, 36\rangle$) has 0.981 (0.981) population probability in band (v) [band (iv)] at time $t = 0$. Figure 6 shows the dynamic evolution from the initial state $|\psi(t_0)\rangle = |21, 35\rangle$ with an evolved time $T_{tot} = 3T_m$. Individual transport is revealed via the particle density distribution $n_j = \langle \psi(t) | \hat{n}_j | \psi(t) \rangle$ in Fig. 6(a) and correlation distribution $R_{ij} = \langle \psi(t) | \hat{a}_i^\dagger \hat{a}_j^\dagger \hat{a}_j \hat{a}_i | \psi(t) \rangle$ in Fig. 6(b). The time evolution of the centroid position is added in Fig. 6(a) with a red line, which reflects the centroid position shifts 2.941 cells after up to $3T_m$. Similar to the independent dynamics in Fig. 6, the initial two bosons mainly occupying band (iii) will freely propagate in the opposite direction due to $C = -3$.

Figure 7 manifests the case of initial state $|\psi(t_0)\rangle = |23, 36\rangle$ with $T_{tot} = 6T_m$. Two bosons propagate toward each other until they occupy nearest-neighbor sites, then are forbidden to stay at the same site due to the strong interaction strength (named interaction blockade), and finally yields a

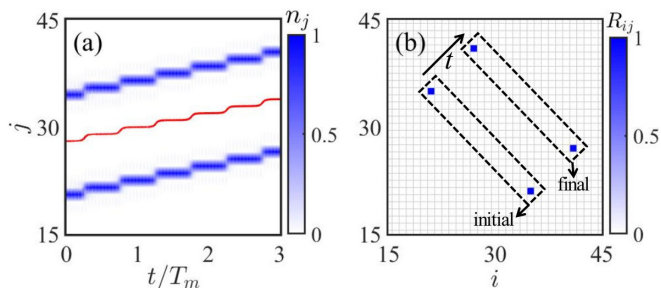


FIG. 6. Topological pumping of scattering states $|\psi(t_0)\rangle = |21, 35\rangle$. (a) The time evolution of the particle density distribution. The center-of-mass position at each moment is shown with a red line. (b) The correlation distribution at moments $t/T_m = 0$ and 3 . The parameters are chosen as $J = -1$, $\delta_0 = 0.8$, $\Delta_0 = 7$, $U = 30$, $\omega = 0.05$, $\phi_0 = 0$, $\omega_F/\omega = 31/3$, $L_t = 58$. The evolution time is $T_{tot} = 3T_m$.

counterpropagating away from each other [see Fig. 7(a)]. After an evolved time $T_{tot} = 6T_m$, the centroid position remains almost constant in Fig. 7(b). Figures 7(c) and 7(d) respectively show the two-boson correlations at moments $t/T_m = 0$ and 3 . During the interaction blockade, the large energy difference coming from the interaction prevents two bosons from binding at the same site while behaving similarly to Fig. 7(d). Finally, two bosons almost return to the initial position as in Fig. 7(c). For $U = 0$, the energy spectrum of two noninteracting bosons consists of three scattering-state bands and two bosons undergo independent dynamics in the absence of an interaction blockade in Appendix E.

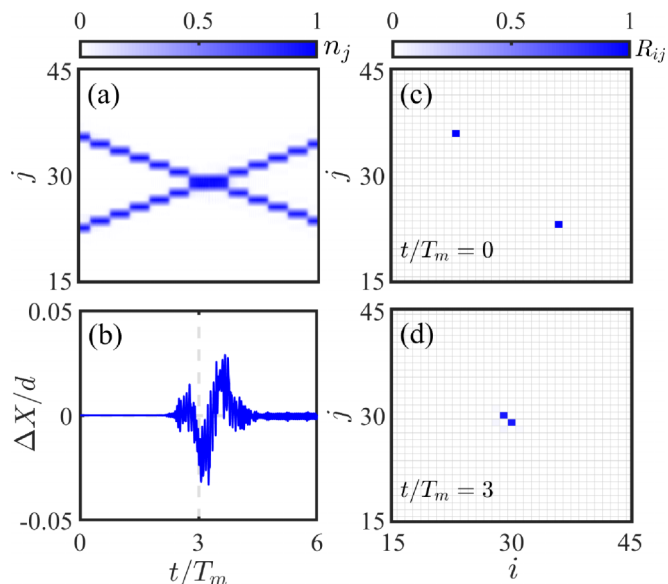


FIG. 7. Topological pumping of scattering states $|\psi(t_0)\rangle = |23, 36\rangle$. The time evolution of the particle density distribution (a) and center-of-mass displacement (b). (c) and (d) are the correlation distributions at moments $t/T_m = 0$ and $t/T_m = 3$. The parameters are chosen as $J = -1$, $\delta_0 = 0.8$, $\Delta_0 = 7$, $U = 30$, $\omega = 0.05$, $\phi_0 = 0$, $\omega_F/\omega = 31/3$, $L_t = 58$. The evolution time is $T_{tot} = 6T_m$.

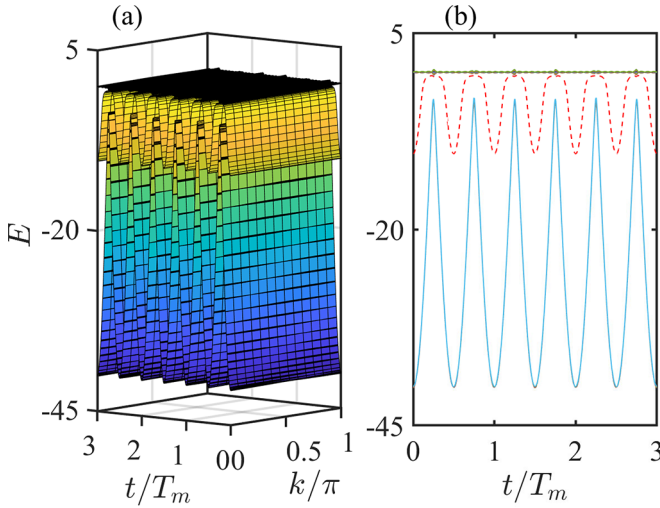


FIG. 8. The lowest three energy bands of two bosons. (a) The 3D view of Bloch bands in the parameter space (k, t) . (b) The time evolution of energies $E(t)$ for Bloch states with $k = 0$. The parameters are chosen as $J = -1$, $\delta_0 = 0.8$, $\Delta_0 = 20$, $U = 30$, $\omega = 0.005$, $\phi_0 = 0$, $\omega_F/\omega = 10/3$, $L_t = 26$.

V. TOPOLOGICALLY RESONANT TUNNELINGS ASSISTED BY BLOCH OSCILLATIONS

Except for the topological transport of bound and scattering states, when $U \gg (J, \delta_0, \omega_F)$ and $\Delta_0 > U/2$ it is expected that topologically resonant tunnelings could be one of typical interaction effects. The interaction strength will match with on-site potential difference between neighboring sites four times over a period T_m , where the two bosons travel one by one rather than as a whole. The effective single-particle model (19) becomes invalid due to the crucial role of coupling between the subspaces \mathcal{U} and \mathcal{V} . Taking the Fock state as an example, once the interaction compensates the on-site potential difference between neighboring sites, resonant tunneling happens between state $|2\rangle_j$ and state $|1\rangle_j|1\rangle_{j+1}$ (or state $|1\rangle_{j-1}|1\rangle_j$) [21].

When the parameters remain the same as those in Fig. 2 except for $\Delta_0 = 20$, the multiparticle Bloch bands are significantly changed, as shown in Fig. 8(a) with the lowest three energy bands. Figure 8(b) shows the change of energies for Bloch states with $k = 0$, where a band marked with a red dashed line is isolated from other bands to allow resonant tunnelings with band Chern number $C = 3$. The energy difference between the states $|1\rangle_j|1\rangle_{j+1}$ and $|2\rangle_j$ (or $|2\rangle_{j+1}$) almost vanishes at the energy avoided crossings. Within a modulation period T_m , four resonant tunnelings occur at four energy avoided crossings.

The multiparticle Bloch state with quasimomentum $k = 0$ is constructed into a Gaussian wave packet as the initial state. The parameters are chosen as $J = -1$, $\delta_0 = 0.8$, $\Delta_0 = 20$, $U = 30$, $\omega = 0.005$, $\phi_0 = 0$, $\omega_F/\omega = 10/3$, and $\sigma = 5$. The system size is $L_t = 74$ and the evolution time is $T_{\text{tot}} = qT_m = 3T_m$. Figure 9(a) exhibits the initial Gaussian wave packet propagates in a certain range whose wave-packet centroid in Fig. 9(b) moves up 2.983 cells after up to $3T_m$. A small deviation from the band Chern number results from non-

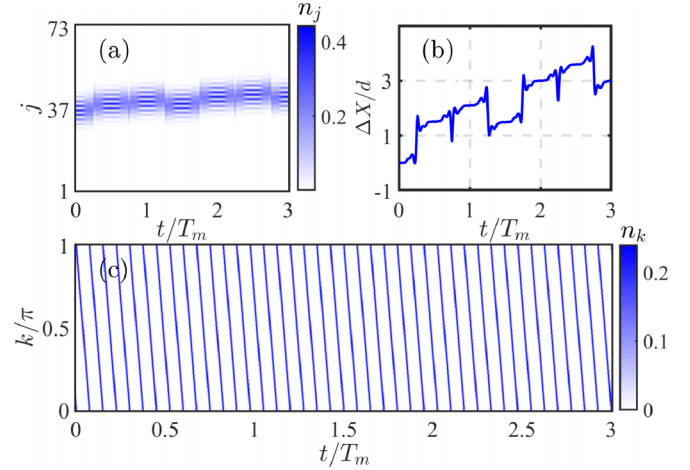


FIG. 9. Topologically resonant tunnelings assisted by Bloch oscillations. (a) and (b) are the time evolution of the particle density distribution in real space and the center-of-mass displacement, respectively. (c) The time evolution of the particle density distribution in quasimomentum space. The parameters are chosen as $J = -1$, $\delta_0 = 0.8$, $\Delta_0 = 20$, $U = 30$, $\omega = 0.005$, $\phi_0 = 0$, $\omega_F/\omega = 10/3$, and $\sigma = 5$. The system size is $L_t = 74$ and the evolution time is $T_{\text{tot}} = qT_m = 3T_m$.

adiabatic transitions due to the slight band gap at the energy avoided crossings. Based on the semiclassical formula (7), we numerically calculate the reduced Chern number of multiparticle Bloch states with quasimomentum $k_0 = 0$, and obtain $C_{\text{red}}(3T_m) = 3$. Both $\Delta X(3T_m)/d$ and $C_{\text{red}}(3T_m)$ approach the band Chern number. Despite a very obvious difference in the real-space density distribution between topologically resonant tunnelings and topological pumping of bound states, the multiparticle center-of-mass momenta both change periodically across the first Brillouin zone and linearly scan the first Brillouin zone at each Bloch-oscillation period [see Fig. 9(c) and Appendix C]. This is because most of the time two bosons stay at the same lattice site as a bound pair, except near the avoided-crossing points. The real-space dynamics of two interacting bosons in tilted optical lattices has been experimentally observed [33]. We find the linear scanning of center-of-mass momentum in the first Brillouin zone at each Bloch-oscillation period, which may provide an effective mean to measure the magnetic field gradient or gravitational field.

VI. SUMMARY AND DISCUSSIONS

We explore the correlated topological pumping by applying a tilted potential in an interacting Rice-Mele model. Attributed to the tilting, the multiparticle center-of-mass momentum changes periodically across the first Brillouin zone and linearly scans the first Brillouin zone at each Bloch-oscillation period. Therefore, it allows us to obtain the information of a multiparticle Bloch band in an entire Brillouin zone even for an initial single-momentum state. Meanwhile, the wave-packet dispersion is suppressed by the tilting. The reduced Chern number defined as a one-dimensional time integral of the Berry curvature characterizes the topological properties of multiparticle Bloch bands. Interaction plays a key role in the emergence of correlated topological pumping. The interaction

binds two bosons together as a pair for topological pumping. By applying the perturbation analysis, the effective single-particle model is derived to explain the behavior of bound states when the interaction is dominated. For scattering states, fruitful topological transports can be engineered by choosing the two-particle initial positions. When two counterpropagating bosons meet at the nearest-neighbor lattice sites, an interaction blockade occurs where interaction prohibits two bosons from crossing each other. The topologically resonant tunnelings in which the two particles move one by one are clarified when the interaction compensates the on-site potential difference between nearest-neighbor sites.

Unlike the single-particle case in Ref. [18], we demonstrate that the multiparticle center-of-mass momentum linearly scans the first Brillouin zone at each Bloch-oscillation period in the presence of a tilted field. The role of the tilting allows one to obtain the information of the multiparticle Bloch band in an entire Brillouin zone even for an initial single-momentum state. This feature can be applied to many-body systems to explore fractional topological states and extract many-body topological invariants.

We focus on repulsive interactions for the correlated topological pumping due to the experimentally observed repulsively bound pairs [49] as well as their coherent dynamics [33]. A symmetry-protected dynamical symmetry theorem establishes a symmetric relation of the time evolution observable between repulsive and attractive systems [50,51]. Naturally, the dynamics of attractive interactions can be directly derived from the corresponding positive one according to such a theorem. Our results are of great significance for topological pumping and can be generalized to topological spin pumping such as two-component bosons where two com-

ponents can be viewed as pseudospin $s = 1/2$ [52,53], and other types of Thouless pumping such as nonlinear Thouless pumping [26,27], non-Abelian Thouless pumping [54–56], fractional Thouless pumping [57], and higher-order topological pumping [58]. Taking the two-component bosons into account, it is possible to obtain a dispersionless topological spin transport with accessible initial states, which has potential applications for designing robust and flexible topological quantum devices, such as topological beam splitters.

ACKNOWLEDGMENTS

We acknowledge useful discussions with Bo Zhu and Zhoutao Lei. This work is supported by the National Natural Science Foundation of China (NSFC) (Grants No. 12025509 and No. 11874434), the Key-Area Research and Development Program of Guangdong Province (Grant No. 2019B030330001), and the Science and Technology Program of Guangzhou (China) (Grant No. 201904020024). W.L. is partially supported by the NSFC (Grant No. 12147108) and the Fundamental Research Funds for the Central Universities, Sun Yat-Sen University (Grant No. 22qntd3101). Y.K. is partially supported by the NSFC (Grants No. 11904419 and No. 12275365). S.H. is partially supported by the NSFC (Grant No. 12104103). L.Z. is partially supported by the Fundamental Research Funds for the Central Universities, Sun Yat-Sen University (Grant No. 22qntd3101).

APPENDIX A: BULK-BOUNDARY CORRESPONDENCE OF MULTIPARTICLE BLOCH BANDS

The bulk-boundary correspondence is a key feature in topological band theory, that is, nontrivial band topology is

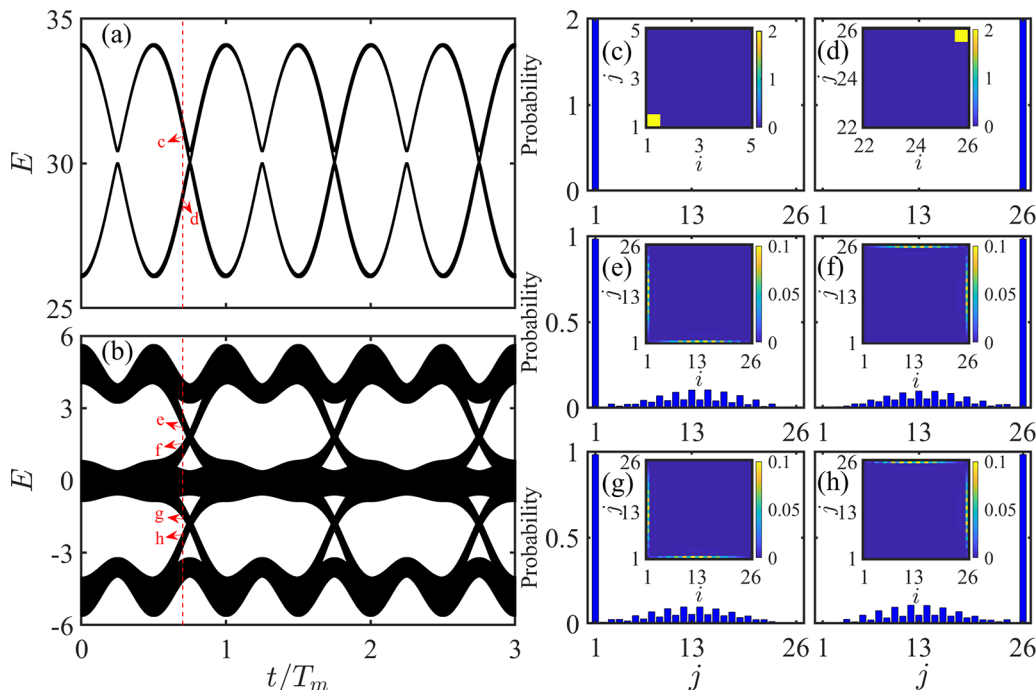


FIG. 10. Two-boson energy spectrum under the open boundary condition. (a) and (b) are the energy spectra as a function of time t . (c)–(h) are the density distributions of chosen states marked with (c)–(h) in red dashed lines in (a) and (b). The insets depict corresponding correlation distributions R_{ij} . The parameters are chosen as $J = -1$, $\delta_0 = 0.8$, $\Delta_0 = 2$, $U = 30$, $\omega = 0.005$, $\phi_0 = 0$, $\omega_F/\omega = 10/3$, $L_t = 26$.

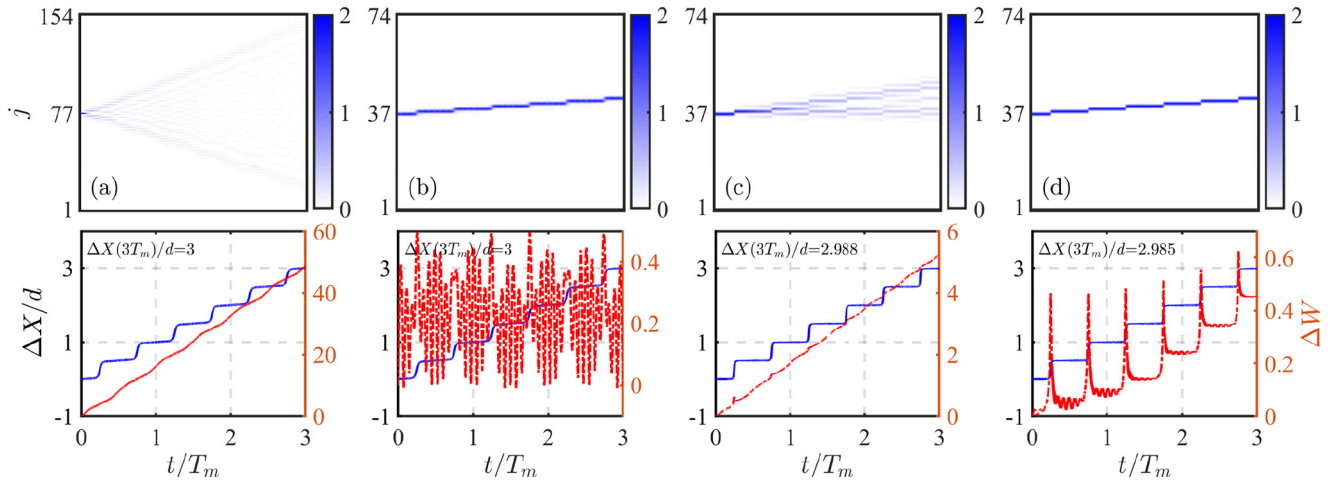


FIG. 11. The time evolution of particle density distribution obtained using initial multiparticle Wannier states. Blue lines and red dashed lines indicate the corresponding center-of-mass displacement $\Delta X(t)/d$ and variation of wave-packet width $\Delta W(t)$. Different interaction strengths are examined: $U = 10$ [(a) and (b)] and $U = 30$ [(c) and (d)]. The role of tilt is analyzed: $\omega_F = 0$ [(a) and (c)] and $\omega_F = 10\omega/3$ [(b) and (d)]. The other parameters are chosen as $J = -1$, $\delta_0 = 0.8$, $\Delta_0 = 2$, $\omega = 0.005$, $\phi_0 = 0$, and $T_{\text{tot}} = qT_m = 3T_m$.

associated with the existence of topological edge states at open boundaries [59,60]. Compared with the multiparticle Bloch band in Fig. 2(a) in the main text, under the open boundary condition isolated states appear at the energy gap in Figs. 10(a) and 10(b). For the chosen parameter marked with red dashed lines in Figs. 10(a) and 10(b), we respectively extract states c–h to compute the density distributions: left (right) two-boson edge state in [Figs. 10(c) and 10(d)] and left (right) single-boson edge states in Figs. 10(e) and 10(g) [Figs. 10(f) and 10(h)]. For bound-state bands, two bosons both stay at the same edge to form two-boson edge states [see Figs. 10(c) and 10(d)]. For scattering-state bands, the interaction prevents two bosons from binding at the same edge due to the large energy difference, while allows one boson at one edge and the other one remains spatially extended along the remaining sites [see Figs. 10(e)–10(h)]. Correlation distributions in the insets show that one-boson edge states are the direct product of a state with one boson locating at one edge and another state with one boson distributing in the bulk sites. Therefore, we classified the states in Figs. 10(e)–10(h) as single-boson edge states.

APPENDIX B: WAVE-PACKET DYNAMICS OF INITIAL MULTIPARTICLE WANNIER STATES

Figure 11 shows the wave-packet dynamics obtained using initial multiparticle Wannier states. The quantized topological pumping requires uniformly filled bands. Fortunately, the multiparticle Wannier state, as an equal superposition of all the multiparticle Bloch states at each quasimomentum, uniformly fills a given band. As seen in Fig. 11, for initial multiparticle Wannier states the center-of-mass displacements are all quantized whether the tilt is present or not. However, the nontrivial role of tilt is able to suppress the wave-packet dispersion. Let us note that a slower driven frequency is required to guarantee quantized transport for a stronger interaction due to the energy gap reduced by interaction. Therefore, the slight deviations from exactly the quantized value in Figs. 11(c)

and 11(d) with $U = 30$ originate from the nonadiabatic effects.

APPENDIX C: DENSITY DISTRIBUTION IN QUASIMOMENTUM SPACE

In the presence of a tilt, it is a challenge in real space to extract the period of the Bloch oscillations. By transferring the evolved states in Figs. 4(g) and 4(h) in the main text to the k -space representation, the average quasimomentum of the wave packet respectively remains unchanged and linearly scans the

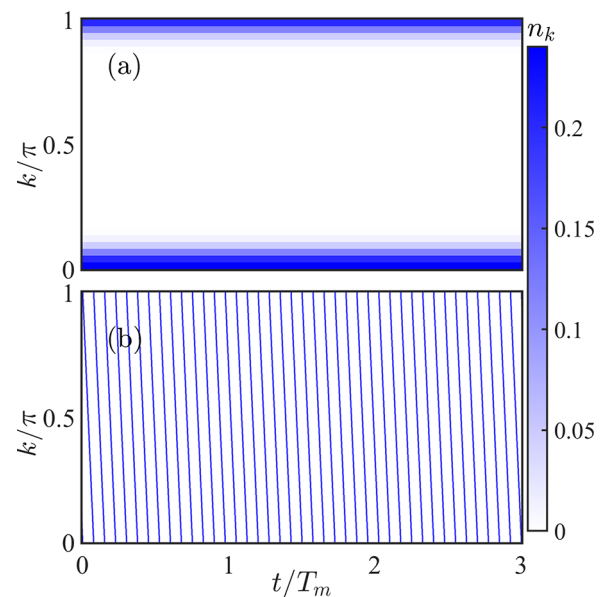


FIG. 12. The time evolution of particle density distribution in quasimomentum space for different values of ω_F : (a) $\omega_F = 0$ and (b) $\omega_F = 10\omega/3$. The other parameters are chosen as $J = -1$, $\delta_0 = 0.8$, $\Delta_0 = 2$, $U = 30$, $\omega = 0.005$, $\phi_0 = 0$, and $\sigma = 5$. The system size is $L_t = 74$ and the evolution time is $T_{\text{tot}} = qT_m = 3T_m$.

first Brillouin zone at each Bloch-oscillation period as time evolves, as shown in Figs. 12(a) and 12(b). Figure 12(b) manifests that when the quasimomentum hits the boundary $k = 0$ in the first Brillouin zone, it immediately transitions to another boundary $k = \pi$. The number of Bloch oscillations can be clearly extracted by counting the number for scanning the first Brillouin zone of the average quasimomentum. It can be seen that the wave packet performs fractional Bloch oscillations with a period half of the single-particle Bloch-oscillation period $T_B = 2\pi/(d\omega_F)$, which means the effective tilt experienced by two strongly interacting bosons turns out to be $2\omega_F$. Naturally, the time evolution of particle density distribution in quasimomentum space can be used to

determine the value of the tilt, which has potential applications in measuring gradient magnetic field or gravitational field.

APPENDIX D: THE RELATIONSHIP BETWEEN REDUCED CHERN NUMBER AND CHERN NUMBER

We prove that the reduced Chern number of bound-state bands $C_{m,\text{red}}$ is independent of the value of quasimomentum, and build its relationship with the Chern number. Based on the analytical expression of the Berry curvature (27) in the main text, it can be seen that in the absence of tilted potential the Berry curvature becomes

$$\mathcal{F}_{\pm}^0(k, t) = 32 \frac{J\delta_0\omega\Delta_0}{U} \frac{\{J^2 + \delta_0^2 \sin^2[\phi(t)]\}}{U} \frac{1 - \cos^2[\phi(t)] \cos^2(k)}{[\varepsilon_{\pm}^0(k, t)]^3}, \quad (\text{D1})$$

where

$$\varepsilon_{\pm}^0(k, t) = \pm \sqrt{\left(4 \frac{\{J^2 + \delta_0^2 \sin^2[\phi(t)]\}}{U} \cos k\right)^2 + \left(4 \frac{\{2J\delta_0 \sin[\phi(t)]\}}{U} \sin k\right)^2 + (2\Delta_0 \cos[\phi(t)])^2 + \mathcal{C}} \quad (\text{D2})$$

is the eigenvalue of the bound-state bands for $\omega_F = 0$. There exist $\varepsilon_{\pm}(k, t) = \varepsilon_{\pm}^0(k - 2\omega_F t, t)$ and $\mathcal{F}_{\pm}(k, t) = \mathcal{F}_{\pm}^0(k - 2\omega_F t, t)$. As k goes to $k + \Delta k$ and t goes to $t + \Delta k/(2\omega_F)$, the Berry curvature yields

$$\begin{aligned} & \mathcal{F}_{\pm}(k + \Delta k, t + \Delta k/2\omega_F) \\ &= \frac{\pm 32J\delta_0\omega\Delta_0 \{J^2 + \delta_0^2 \sin^2[\phi(t) + \phi_s]\} \{1 - \cos^2[\phi(t) + \phi_s] \cos^2(k - 2\omega_F t)\}}{U^2 \left\{ \left[4 \frac{\{J^2 + \delta_0^2 \sin^2[\phi(t) + \phi_s]\}}{U} \cos(k - 2\omega_F t) \right]^2 + \left[4 \frac{\{2J\delta_0 \sin[\phi(t) + \phi_s]\}}{U} \sin(k - 2\omega_F t) \right]^2 + [2\Delta_0 \cos[\phi(t) + \phi_s]]^2 \right\}^{3/2}} \\ &\approx \frac{\pm 32J\delta_0\omega\Delta_0 \{J^2 + \delta_0^2 \sin^2[\phi(t)]\} \{1 - \cos^2[\phi(t)] \cos^2(k - 2\omega_F t)\}}{U^2 \left\{ \left[4 \frac{\{J^2 + \delta_0^2 \sin^2[\phi(t)]\}}{U} \cos(k - 2\omega_F t) \right]^2 + \left[4 \frac{\{2J\delta_0 \sin[\phi(t)]\}}{U} \sin(k - 2\omega_F t) \right]^2 + [2\Delta_0 \cos \phi(t)]^2 \right\}^{3/2}} \\ &= \mathcal{F}_{\pm}^0(k, t) \end{aligned} \quad (\text{D3})$$

with $\phi_s = \frac{\omega}{2\omega_F} \Delta k$. When $\omega_F/\omega \rightarrow \infty$, we have $\phi_s = 0$ and the relation (D3) becomes exact enough. In the following derivation, we assume that the system respects $\omega_F/\omega \rightarrow \infty$. Since the Berry curvature (D3) is a periodic function with period qT_m in time domain, the one-dimensional time integral of the Berry curvature (D3) follows:

$$\begin{aligned} & \int_0^{qT_m} \mathcal{F}_{\pm}(k + \Delta k, t + \Delta k/2\omega_F) \\ & dt = \int_{\Delta k/2\omega_F}^{qT_m + \Delta k/2\omega_F} \mathcal{F}_{\pm}(k + \Delta k, t) \\ & dt = \int_0^{qT_m} \mathcal{F}_{\pm}(k + \Delta k, t) dt. \end{aligned} \quad (\text{D4})$$

According to Eqs. (D3) and (D4), we have

$$C_{m,\text{red}} = \frac{1}{d} \int_0^{qT_m} \mathcal{F}_{\pm}(k, t) dt = \frac{1}{d} \int_0^{qT_m} \mathcal{F}_{\pm}(k + \Delta k, t) dt. \quad (\text{D5})$$

It means that the reduced Chern number of bound-state bands $C_{m,\text{red}}$ is independent of the value of quasimomentum k

with

$$C_{m,\text{red}}(k + \Delta k) = C_{m,\text{red}}(k). \quad (\text{D6})$$

Thus, we can average the reduced Chern number over the first Brillouin zone without affecting the final results as

$$\begin{aligned} C_{m,\text{red}}(qT_m) &= \frac{1}{2\pi} \int_0^{qT_m} \int_{-\pi/d}^{\pi/d} \mathcal{F}_m^0(k - 2\omega_F t, t) dt dk \\ &= \frac{1}{2\pi} \int_0^{qT_m} \int_{-\pi/d}^{\pi/d} \mathcal{F}_m^0(k, t) dt dk = C_m. \end{aligned} \quad (\text{D7})$$

Unlike the Chern number obtained by a two-dimensional integral, the reduced Chern number is a one-dimensional integral over time. The reason is that in the presence of a tilt, all quasimomentum values are uniformly sampled over a time cycle. The quasimomentum sampling can be understood as a valid ergodic behavior in the Brillouin zone, such that the

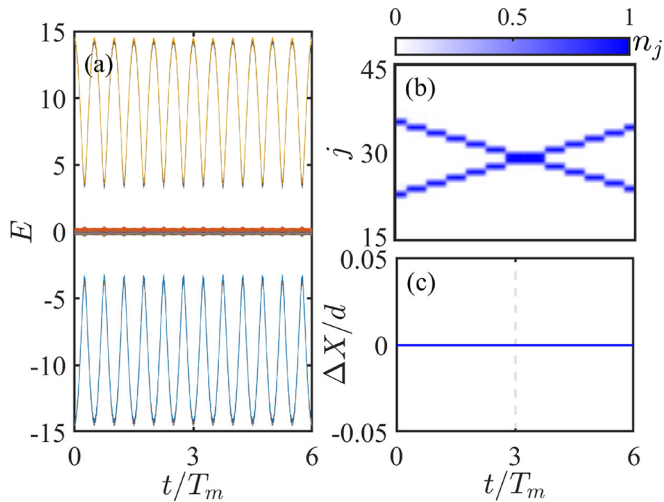


FIG. 13. Two noninteracting bosons. (a) The time evolution of energies $E(t)$ for Bloch states with $k = 0$. Topological pumping of scattering states $|\psi(t_0)\rangle = |23, 36\rangle$: the time evolution of the particle density distribution (b) and center-of-mass displacement (c). The parameters are chosen as $J = -1$, $\delta_0 = 0.8$, $\Delta_0 = 7$, $U = 0$, $\omega = 0.05$, $\phi_0 = 0$, $\omega_F/\omega = 31/3$, $L_t = 58$. The evolution time is $T_{\text{tot}} = 6T_m$.

one-dimensional time integral is independent of the specific value of the initial quasimomentum k_0 .

APPENDIX E: TWO NONINTERACTING BOSONS IN A PERIODICALLY DRIVEN AND TILTED SUPERLATTICE

When $U = 0$, the two-boson energy spectrum just consists of three scattering-state bands and Fig. 13(a) exhibits its change for Bloch states with $k = 0$ as time evolves. The upper and lower multiparticle Bloch bands belong to topologically nontrivial scattering-state bands with Chern number $C = -3$ and $C = 3$, respectively. The middle band is topologically trivial with $C = 0$. When the two noninteracting bosons are far away from each other and occupy the topologically nontrivial scattering-state bands, the two bosons as a Fock state can be transferred as a whole similar to the interacting case in Fig. 6. When the two bosons are initially prepared on the topologically trivial scattering-state bands, the two counterpropagating bosons can be independently shifted toward each other, and come back to the initial state after crossing each other without an interaction blockade in Fig. 13(b). Unlike the interaction blockade in Fig. 7, two bosons undergo independent dynamics whose center-of-mass displacement always remains zero, as shown in Fig. 13(c).

- [1] D. J. Thouless, Quantization of particle transport, *Phys. Rev. B* **27**, 6083 (1983).
- [2] Q. Niu and D. J. Thouless, Quantised adiabatic charge transport in the presence of substrate disorder and many-body interaction, *J. Phys. A: Math. Gen.* **17**, 2453 (1984).
- [3] J. P. Pekola, O.-P. Saira, V. F. Maisi, A. Kemppinen, M. Möttönen, Y. A. Pashkin, and D. V. Averin, Single-electron current sources: Toward a refined definition of the ampere, *Rev. Mod. Phys.* **85**, 1421 (2013).
- [4] Y. Ke, X. Qin, F. Mei, H. Zhong, Y. S. Kivshar, and C. Lee, Topological phase transitions and Thouless pumping of light in photonic waveguide arrays, *Laser Photonics Rev.* **10**, 995 (2016).
- [5] S. Hu, Y. Ke, Y. Deng, and C. Lee, Dispersion-suppressed topological Thouless pumping, *Phys. Rev. B* **100**, 064302 (2019).
- [6] S. Hu, Y. Ke, and C. Lee, Topological quantum transport and spatial entanglement distribution via a disordered bulk channel, *Phys. Rev. A* **101**, 052323 (2020).
- [7] K. J. M. Schouten and V. Cheianov, Rapid-cycle Thouless pumping in a one-dimensional optical lattice, *Phys. Rev. A* **104**, 063315 (2021).
- [8] S. Malikis and V. Cheianov, An ideal rapid-cycle Thouless pump, *SciPost Phys.* **12**, 203 (2022).
- [9] M. Lohse, C. Schweizer, O. Zilberberg, M. Aidelsburger, and I. Bloch, A Thouless quantum pump with ultracold bosonic atoms in an optical superlattice, *Nat. Phys.* **12**, 350 (2016).
- [10] S. Nakajima, T. Tomita, S. Taie, T. Ichinose, H. Ozawa, L. Wang, M. Troyer, and Y. Takahashi, Topological Thouless pumping of ultracold fermions, *Nat. Phys.* **12**, 296 (2016).
- [11] M. Lohse, C. Schweizer, H. M. Price, O. Zilberberg, and I. Bloch, Exploring 4D quantum Hall physics with a 2D topological charge pump, *Nature (London)* **553**, 55 (2018).
- [12] S. Nakajima, N. Takei, K. Sakuma, Y. Kuno, P. Marra, and Y. Takahashi, Competition and interplay between topology and quasi-periodic disorder in Thouless pumping of ultracold atoms, *Nat. Phys.* **17**, 844 (2021).
- [13] Y. E. Kraus, Y. Lahini, Z. Ringel, M. Verbin, and O. Zilberberg, Topological States and Adiabatic Pumping in Quasicrystals, *Phys. Rev. Lett.* **109**, 106402 (2012).
- [14] O. Zilberberg, S. Huang, J. Guglielmon, M. Wang, K. P. Chen, Y. E. Kraus, and M. C. Rechtsman, Photonic topological boundary pumping as a probe of 4D quantum Hall physics, *Nature (London)* **553**, 59 (2018).
- [15] A. Cerjan, M. Wang, S. Huang, K. P. Chen, and M. C. Rechtsman, Thouless pumping in disordered photonic systems, *Light Sci. Appl.* **9**, 178 (2020).
- [16] W. Ma, L. Zhou, Q. Zhang, M. Li, C. Cheng, J. Geng, X. Rong, F. Shi, J. Gong, and J. Du, Experimental Observation of a Generalized Thouless Pump with a Single Spin, *Phys. Rev. Lett.* **120**, 120501 (2018).
- [17] H.-I. Lu, M. Schemmer, L. M. Aycock, D. Genkina, S. Sugawa, and I. B. Spielman, Geometrical Pumping with a Bose-Einstein Condensate, *Phys. Rev. Lett.* **116**, 200402 (2016).
- [18] Y. Ke, S. Hu, B. Zhu, J. Gong, Y. Kivshar, and C. Lee, Topological pumping assisted by Bloch oscillations, *Phys. Rev. Res.* **2**, 033143 (2020).
- [19] J. Tangpanitanon, V. M. Bastidas, S. Al-Assam, P. Roushan, D. Jaksch, and D. G. Angelakis, Topological Pumping of Photons in Nonlinear Resonator Arrays, *Phys. Rev. Lett.* **117**, 213603 (2016).
- [20] L. Lin, Y. Ke, and C. Lee, Interaction-induced topological bound states and Thouless pumping in a one-dimensional optical lattice, *Phys. Rev. A* **101**, 023620 (2020).

- [21] Y. Ke, X. Qin, Y. S. Kivshar, and C. Lee, Multiparticle Wannier states and Thouless pumping of interacting bosons, *Phys. Rev. A* **95**, 063630 (2017).
- [22] X. Liu, S. Tan, Q. hai Wang, L. Zhou, and J. Gong, Floquet band engineering with Bloch oscillations, *Phys. Rev. B* **106**, 224309 (2022).
- [23] A. Hayward, C. Schweizer, M. Lohse, M. Aidelsburger, and F. Heidrich-Meisner, Topological charge pumping in the interacting bosonic Rice-Mele model, *Phys. Rev. B* **98**, 245148 (2018).
- [24] S. Greschner, S. Mondal, and T. Mishra, Topological charge pumping of bound bosonic pairs, *Phys. Rev. A* **101**, 053630 (2020).
- [25] A.-S. Walter, Z. Zhu, M. Gächter, J. Minguzzi, S. Roschinski, K. Sandholzer, K. Viebahn, and T. Esslinger, Breakdown of quantisation in a Hubbard-Thouless pump, [arXiv:2204.06561](https://arxiv.org/abs/2204.06561) v1.
- [26] M. Jürgensen, S. Mukherjee, and M. C. Rechtsman, Quantized nonlinear Thouless pumping, *Nature (London)* **596**, 63 (2021).
- [27] Q. Fu, P. Wang, Y. V. Kartashov, V. V. Konotop, and F. Ye, Non-linear Thouless Pumping: Solitons and Transport Breakdown, *Phys. Rev. Lett.* **128**, 154101 (2022).
- [28] A. Widera, O. Mandel, M. Greiner, S. Kreim, T. W. Hänsch, and I. Bloch, Entanglement Interferometry for Precision Measurement of Atomic Scattering Properties, *Phys. Rev. Lett.* **92**, 160406 (2004).
- [29] C. Gross, T. Zibold, E. Nicklas, J. Estève, and M. K. Oberthaler, Nonlinear atom interferometer surpasses classical precision limit, *Nature (London)* **464**, 1165 (2010).
- [30] D. M. Weld, P. Medley, H. Miyake, D. Hucul, D. E. Pritchard, and W. Ketterle, Spin Gradient Thermometry for Ultracold Atoms in Optical Lattices, *Phys. Rev. Lett.* **103**, 245301 (2009).
- [31] M. Karski, L. Förster, J.-M. Choi, A. Steffen, N. Belmechri, W. Alt, D. Meschede, and A. Widera, Imprinting patterns of neutral atoms in an optical lattice using magnetic resonance techniques, *New J. Phys.* **12**, 065027 (2010).
- [32] G. Jotzu, M. Messer, F. Görg, D. Greif, R. Desbuquois, and T. Esslinger, Creating State-Dependent Lattices for Ultracold Fermions by Magnetic Gradient Modulation, *Phys. Rev. Lett.* **115**, 073002 (2015).
- [33] P. M. Preiss, R. Ma, M. E. Tai, A. Lukin, M. Rispoli, P. Zupancic, Y. Lahini, R. Islam, and M. Greiner, Strongly correlated quantum walks in optical lattices, *Science* **347**, 1229 (2015).
- [34] Z. A. Geiger, K. M. Fujiwara, K. Singh, R. Senaratne, S. V. Rajagopal, M. Lipatov, T. Shimasaki, R. Driben, V. V. Konotop, T. Meier, and D. M. Weld, Observation and Uses of Position-Space Bloch Oscillations in an Ultracold Gas, *Phys. Rev. Lett.* **120**, 213201 (2018).
- [35] H. Kim, G. Zhu, J. V. Porto, and M. Hafezi, Optical Lattice with Torus Topology, *Phys. Rev. Lett.* **121**, 133002 (2018).
- [36] G. Ferrari, N. Poli, F. Sorrentino, and G. M. Tino, Long-Lived Bloch Oscillations with Bosonic Sr Atoms and Application to Gravity Measurement at the Micrometer Scale, *Phys. Rev. Lett.* **97**, 060402 (2006).
- [37] N. Poli, F.-Y. Wang, M. G. Tarallo, A. Alberti, M. Prevedelli, and G. M. Tino, Precision Measurement of Gravity with Cold Atoms in an Optical Lattice and Comparison with a Classical Gravimeter, *Phys. Rev. Lett.* **106**, 038501 (2011).
- [38] J. Motruk and I. Na, Detecting Fractional Chern Insulators in Optical Lattices Through Quantized Displacement, *Phys. Rev. Lett.* **125**, 236401 (2020).
- [39] C. Repellin, J. Léonard, and N. Goldman, Fractional Chern insulators of few bosons in a box: Hall plateaus from center-of-mass drifts and density profiles, *Phys. Rev. A* **102**, 063316 (2020).
- [40] B. Zhu, S. Hu, H. Zhong, and Y. Ke, Uncovering band topology via quantized drift in two-dimensional Bloch oscillations, *Phys. Rev. B* **104**, 104314 (2021).
- [41] A. R. Kolovsky and A. Buchleitner, Floquet-Bloch operator for the Bose-Hubbard model with static field, *Phys. Rev. E* **68**, 056213 (2003).
- [42] L.-J. Lang, X. Cai, and S. Chen, Edge States and Topological Phases in One-Dimensional Optical Superlattices, *Phys. Rev. Lett.* **108**, 220401 (2012).
- [43] S.-L. Zhu, Z.-D. Wang, Y.-H. Chan, and L.-M. Duan, Topological Bose-Mott Insulators in a One-Dimensional Optical Superlattice, *Phys. Rev. Lett.* **110**, 075303 (2013).
- [44] D. J. Thouless, M. Kohmoto, M. P. Nightingale, and M. den Nijs, Quantized Hall Conductance in a Two-Dimensional Periodic Potential, *Phys. Rev. Lett.* **49**, 405 (1982).
- [45] D. Xiao, M.-C. Chang, and Q. Niu, Berry phase effects on electronic properties, *Rev. Mod. Phys.* **82**, 1959 (2010).
- [46] Z. Fedorova, H. Qiu, S. Linden, and J. Kroha, Observation of topological transport quantization by dissipation in fast Thouless pumps, *Nat. Commun.* **11**, 3758 (2020).
- [47] M. Takahashi, Half-filled Hubbard model at low temperature, *J. Phys. C* **10**, 1289 (1977).
- [48] S. Bravyi, D. P. DiVincenzo, and D. Loss, Schrieffer-Wolff transformation for quantum many-body systems, *Ann. Phys.* **326**, 2793 (2011).
- [49] K. Winkler, G. Thalhammer, F. Lang, R. Grimm, J. H. Denschlag, A. J. Daley, A. Kantian, H. P. Büchler, and P. Zoller, Repulsively bound atom pairs in an optical lattice, *Nature (London)* **441**, 853 (2006).
- [50] J. Yu, N. Sun, and H. Zhai, Symmetry Protected Dynamical Symmetry in the Generalized Hubbard Models, *Phys. Rev. Lett.* **119**, 225302 (2017).
- [51] W. Liu, Y. Ke, L. Zhang, and C. Lee, Bloch oscillations of multimagnon excitations in a Heisenberg XXZ chain, *Phys. Rev. A* **99**, 063614 (2019).
- [52] O. Mandel, M. Greiner, A. Widera, T. Rom, T. W. Hänsch, and I. Bloch, Coherent Transport of Neutral Atoms in Spin-Dependent Optical Lattice Potentials, *Phys. Rev. Lett.* **91**, 010407 (2003).
- [53] C. Schweizer, M. Lohse, R. Citro, and I. Bloch, Spin Pumping and Measurement of Spin Currents in Optical Superlattices, *Phys. Rev. Lett.* **117**, 170405 (2016).
- [54] V. Broscio, L. Piloizzi, R. Fazio, and C. Conti, Non-Abelian Thouless pumping in a photonic lattice, *Phys. Rev. A* **103**, 063518 (2021).
- [55] O. You, S. Liang, B. Xie, W. Gao, W. Ye, J. Zhu, and S. Zhang, Observation of Non-Abelian Thouless Pump, *Phys. Rev. Lett.* **128**, 244302 (2022).
- [56] Y.-K. Sun, X.-L. Zhang, F. Yu, Z.-N. Tian, Q.-D. Chen, and H.-B. Sun, Non-Abelian Thouless pumping in photonic waveguides, *Nat. Phys.* **18**, 1080 (2022).

- [57] M. Jürgensen, S. Mukherjee, C. Jörg, and M. C. Rechtsman, Quantized fractional Thouless pumping of solitons, [arXiv:2201.08258](https://arxiv.org/abs/2201.08258).
- [58] W. A. Benalcazar, J. Noh, M. Wang, S. Huang, K. P. Chen, and M. C. Rechtsman, Higher-order topological pumping and its observation in photonic lattices, *Phys. Rev. B* **105**, 195129 (2022).
- [59] Y. Hatsugai, Edge states in the integer quantum Hall effect and the Riemann surface of the Bloch function, *Phys. Rev. B* **48**, 11851 (1993).
- [60] Y. Hatsugai, Chern Number and Edge States in the Integer Quantum Hall Effect, *Phys. Rev. Lett.* **71**, 3697 (1993).